

STUDY THE EFFECTS OF SINTERING TEMPERATURE TO $Zn_{0.45}Mn_{0.55}Fe_2O_4$ NANO FERRITE AND ENHANCE STRUCTURE, MAGNETIC, AND ELECTRICAL PROPERTIES

Muthana El ttayef Abbas

Iraq, University of Diyala, College of Science, Department of Physics

Zena Mohammed Ali abbas

Iraq, University of Diyala, College of Science, Department of Physics

*Corresponding author

E-mail: zenaalbana@yahoo.com ; ffamu55@gmail.com

Abstract

Mn-Zn- Fe_2O_4 ferrites nanoparticles (NPs) prepared via the sol-gel method at 650, 750, and 850 °C must be able to manage the structural, magnetic and electrical characteristics of Mn-Zn-ferrites nanocomposite in order for the nanomaterials to be used. This article describes an investigation into the feasibility of creating Mn-Zn-ferrites (NPs) through sol-gel as potential structure-tailorable nanomaterials. XRD, FE-SEM analysis, Vibrating Sample Magnetometer (VSM), and the electrical (LCR) meter analysis were used to describe the structural and magnetic properties of the Mn-Zn-ferrites using sol-gel method. The crystallite sizes range from 15 to 18 nm, and the cubic structure of the ferrites shows up in XRD (NPs). Nanoparticles having a particle size of 27.77 to 72.04 nm were found in the produced Mn-Zn-ferrites. In the case of the Mn-Zn-ferrites, prominent the VSM demonstrated that the magnetic nature of materials changed dramatically from pristine as magnetization rose and coercivity decreased with Mn-Zn-ferrites nanoparticles. Finally, an optimal magnetic parameter value ($M_s = 0.80$ emu/g and $H_c = 75$ Oe) at (850) °C was obtained from the data.

Keywords: Mn-Zn- Fe_2O_4 NPs; Structural and Magnetic properties; Sol-gel method.

1. Introduction

Establishing environment friendly nano-particulate technology will be a welcome step in the modern scientific era. Many researches that concern with nanotechnology aimed to create a new material with different physical methods. In contrast to bulk materials, nanoparticles (NPs) are microscopic particles with



a diameter of less than 100 nm, synthesized from inorganic or organic materials, and exhibiting novel features. [1]. These NPs include Mn-Zn-Fe₂O₄ NPs, which, when compared to other materials, have considerable advantages in the future [2]. Low toxicity, strong catalytic activity, and compact sizes are only a few of the unique physiochemical features available [3-5]. It has been shown that the cationic distribution and thermal behavior of oxygen are closely linked in manganese zinc ferrite nanocomposite preparations prepared by ceramic methods such as sol-gel [7]. This means that the microstructure and its physical properties are highly dependent on the atmosphere and heat treatment temperatures for these nanocomposite materials [8-10]. The research team has reached an investment of these materials which constitutes a large proportion in the world, in a new research that is not covered yet by any research group to study the structure, magnetic, and electrical properties, the originality of this work is that all of the materials employed (which, to the best of the authors' knowledge, with no consideration given to the expense of producing precious and useful nanoparticle materials. Furthermore, there are no chemical components present in either the raw materials or the finished product at all. In any of the ingredients utilized, there are no additives or preservatives to be found.

In spite of this, the correct controls for sol-gel synthesis may yield monodisperse nanoparticles with good crystallinity, and it is a feasible solution with considerable economic and technological advantages as well as outstanding reproducibility [11-14]. The (Mn-Zn-Fe₂O₄) nanocomposite was characterized and the results were compared to the JCPDS card data using XRD analysis (XRD-6000/Japan) (Joint Committee on Powder Diffraction Standards). The orientation of (Mn-Zn-Fe₂O₄) nanocomposite generated samples was evaluated using XRD measurements in Iraq's Nanotechnology and Advanced Materials/Materials Research Department/Ministry of Science and Technology. Iran-Mashhad "Tescan Mira3 FE-SEM-Czech" used FE-SEM to study the morphology and particle size of its samples (Mn-Zn-Fe₂O₄). It was used to explore the functions group and vibrations modes using a potassium bromide (KBr) beam splitter and a mid IR TGC detector for the polarized reflectance of the IR polarization. This was done using an MPMS XL, a Quantum Design SQUID magnetometer from VSM, the electrical properties (LCR) meter for testing.



2. The Experimental Work

2.1 Method and Materials

The materials used in the preparation of the ferrite compound by sol-gel auto combustion method. Iron (III) nitrate ($\text{Fe}(\text{NO}_3)_3 \cdot 9\text{H}_2\text{O}$) salt, Ammonia solution (NH_3) (Sigma-Aldrich, India, Purity (97.99%)), Citric acid ($\text{C}_6\text{H}_8\text{O}_7 \cdot \text{H}_2\text{O}$), and from a local market, Sigma-Aldrich, India's $\text{Zn}(\text{NO}_3)_2 \cdot 6\text{H}_2\text{O}$ was purchased with a purity of 99.99 % (Baghdad, Iraq). All of the solutions were made with water that had been distilled using a water distiller (Gallenkamp, England). A local market in Baghdad, Iraq, sells manganese (II) nitrate ($\text{Mn}(\text{NO}_3)_2 \cdot 4\text{H}_2\text{O}$), sold by Sigma-Aldrich and purified to 99.99% purity).

2.2 The Synthesized of Mn-Zn- Fe_2O_4 Nanoparticles

In order to dissolve the metal nitrate and citric acid, 15 mL of distilled water was used. They're all mixed together in a glass beaker to come up with one final answer. It takes a magnetic stirrer that moves at high speeds to mix the solution at room temperature until it is smooth and slimy red-colored, as shown in the picture (1a). Dropping ammonia into the mixed solution was how it was done. The solution was stirred all the time to keep the pH level stable until it reached (7), as shown in the figure (1 b). Stir the ingredients together for half an hour at room temperature to make sure they are all the same color. In small steps, raise the temperature until it reaches 90 °C. Keep stirring until the gel form is reached. If you stir the solution in the beaker glass for 30 minutes at 90 °C, you can see a gel-like substance on top of the solution. This is shown in Figure 3. (1 c). This is because the solution is very thick and because it is still on the magnetic stirrer and in the beaker glass at this point. After the solution turns to gel, the gel dries, and the color changes to dark brown, the temperature goes down to room temperature. There are many ways to dry and lower the gel's weight in an oven at 150°C for three hours: (1d). Some of the substance evaporated and the temperature was raised to (250°C), so the dry gel started to convex in a beaker after 15 minutes. The figure shows how it looked (1 e). Following a fire, the dried gel turns into a fine powder with a dark gray tint, which means that high purity ferrite production has begun, as shown in the photo (1f). Finally, the spinel was heated for three hours at (650, 750, and 850 °C) to improve crystallization and uniform action distribution, and then ground to make $\text{Zn}_x\text{Mn}_{1-x}\text{Fe}_2\text{O}_4$ nano powder. The traditional way to make ceramics is to mix titanium dioxide with zinc-manganese ferrite at 500°C in different amounts.

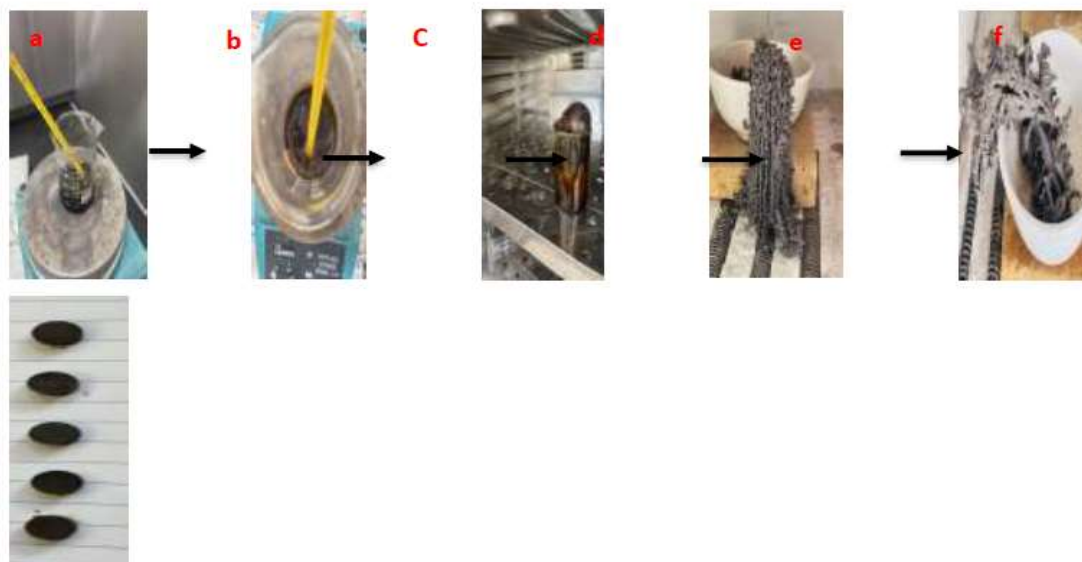


Figure (1): Photograph of (a) nitrates-citrate solution, (b) The solution after the Adding of ammonia, (c) dry gel, (d) Dry bulk temperature of 150°C, (e) Dry bulk temperature of 250°C and (f) auto combustion and become Nano powder ferrite.

3. Results and disscation

3.1 X-ray Diffraction (XRD) of the Mn-Zn- Fe_2O_4 Nanoparticles

XRD is a suitable technique commonly applied to discuss the structural properties to ascertain the crystalline nature and phase identification of pure (Mn-Zn- Fe_2O_4 nanoparticles) nano crystalline powder. From figure 4-5 observed that at the concentration of zinc metal ($x=0.45$), a pure single-phase cubic spinel $\text{Zn}_x\text{Mn}_{1-x}\text{Fe}_2\text{O}_4$ structure was obtained with space group (Fd-3m no. 277), crystal dimensions ($a = b = c = 8.438 \text{ \AA}$) and crystal angles ($\alpha = \beta = \gamma = 90^\circ$), agreed with the standard data (JCPDS 98-017-0912) as shown in figure 2 and table 1. The XRD patterns at high calcination temperatures 750 and 850 °C demonstrated that the distinct structural stability of obtained $\text{Zn}_x\text{Mn}_{1-x}\text{Fe}_2\text{O}_4$ during the calcination process leads to crystalline growth in the same cubic $\text{Zn}_x\text{Mn}_{1-x}\text{Fe}_2\text{O}_4$ structure with a high purity phase, no other impurities peaks were detected, this is an indication that all the reactant metal ions entered into the cubic $\text{Zn}_x\text{Mn}_{1-x}\text{Fe}_2\text{O}_4$ structure at the concentration of zinc metal ($x=0.45$) [15]. The lattice constant value as of pure cubic $\text{Zn}_x\text{Mn}_{1-x}\text{Fe}_2\text{O}_4$ ferrite nanocomposite is reduced when Zn metal added which can be explained on the basis of cations distribution, as a result of replacing larger ionic radii of Mn^{2+} cations (0.082 nm) by smaller ionic radii of Zn^{2+} cations (0.074 nm) [16-17].

The crystallite size (D) was determined by use the Scherer's formula [15]:

$$D \text{ (nm)} = \frac{0.9\lambda}{\beta \cos(\theta)} \tag{1}$$

When, k represents form operator (0.9), λ is represent wavelength (0.15418) nm (CuK α), β is represent Full Width at Half Maximum (FWHM) and θ is represent diffraction angle [15].

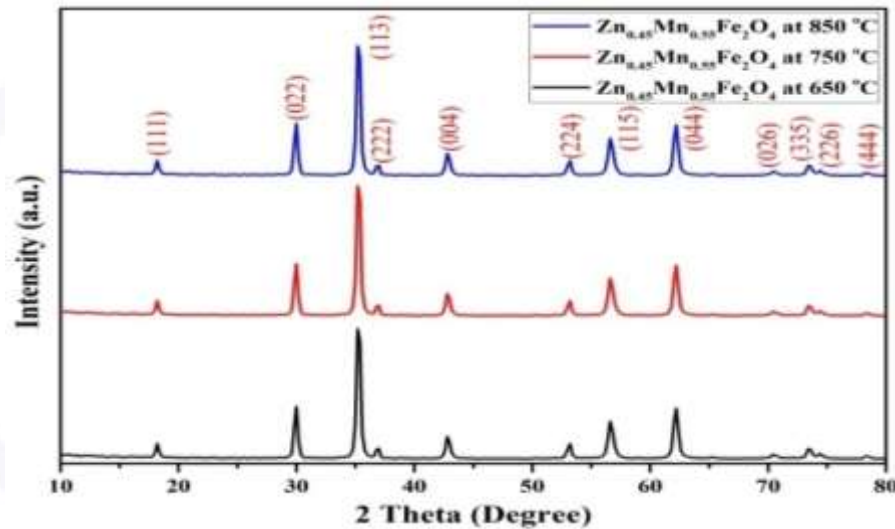


Figure (2): XRD patterns of Zn_{0.45}Mn_{0.55}Fe₂O₄ ferrite nanocomposites at different calcination temperatures (650, 750, 850 °C).

Table 1 XRD calculations of Zn_xMn_{1-x}Fe₂O₄ with different content of zinc metal at different calcination temperatures.

Material	Temp. °C	2θ (deg) Practical	2θ (deg) Standard	FWHM (deg)	Crystalline size (nm)	d _{hkl} (°A) Practical	d _{hkl} (°A) Standard	(hkl)
Zn _{0.45} Mn _{0.55} Fe ₂ O ₄	650	35.27	35.24	0.2704	27.99	2.5443	2.5441	(113)
	750	35.27	35.24	0.2604	29.07	2.5443	2.5441	(113)
	850	35.27	35.24	0.2462	30.77	2.5376	2.5441	(113)

3.2 (FE-SEM) analysis of the Mn-Zn- Fe₂O₄ nanoparticles.

The results of FE-SEM tests on the combination Zn_xMn_{1-x}Fe₂O₄ revealed that the particles had a spherical shape with a limited distribution of nanoparticle sizes, suggesting that the particles were created and have porosity. We also see the fine spherical particles forming a homogenous agglomeration, since particles of smaller size have persistent magnetism, hence each particle has permanent

magnetization as a result of particle agglomeration and grouping. Figures (3) show the results of FE-SEM tests for values ($x= 0.45$) at temperatures (650, 750, and 850 °C), respectively, and show that particle size increases with increasing temperature across the forms. Table 2 shows the estimated diameters of $Zn_xMn_{1-x}Fe_2O_4$ nanoparticles ($x= 0.45$) for calcined specimens at 650, 750, and 850 °C with relatively well-crystallized grains and a mean particle size lower than range from 45 to 97 nm respectively, measured by Image J Software (version 1.51j8; National Institutes of Health, Bethesda, USA).

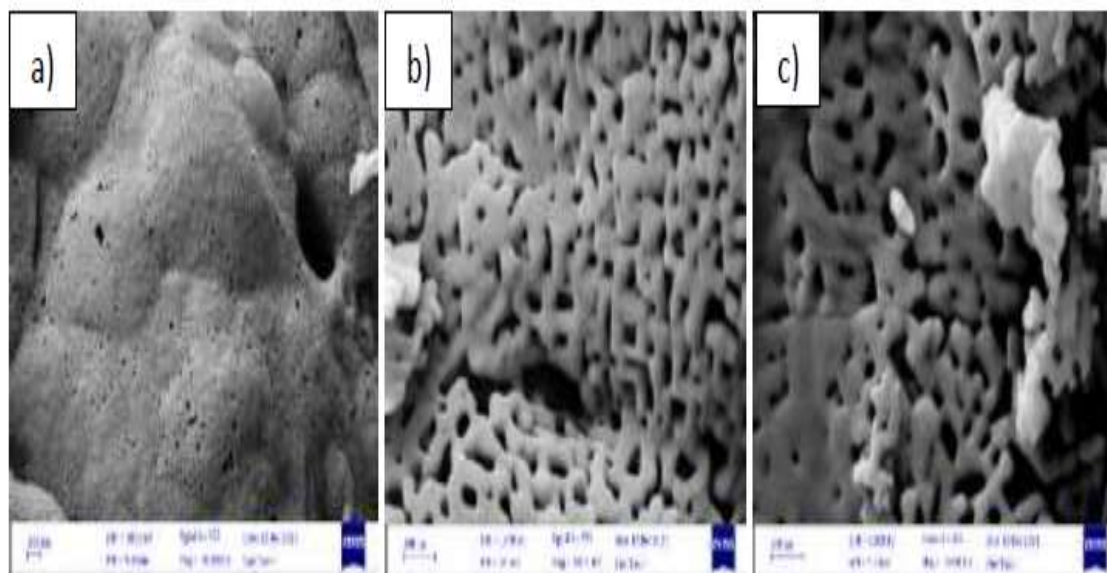


Figure 3: FE-SEM micrographs of $Zn_{0.45}Mn_{0.55}Fe_2O_4$ nanoferrites for (a) calcined specimen at 650 °C (b) at 750 °C and (c) at 850 °C.

3.3 VSM Analysis of the Mn-Zn- Fe_2O_4 Nanoparticles

The magnetic characteristics of the produced samples have been evaluated at room temperature using a vibrating sample magnetometer (VSM) in the applied field ranging of -15 to $+15$ kOe. Hysteresis plots illustrating the variation of magnetization (M_s , emu/g) as a function of applied magnetic field (H , Oe) were plotted for produced nanocrystalline $Mn_xZn_{1-x}Fe_2O_4$ ($x = 0.45$) powders are shown in figure (Figure 4) and table (2). Mn-Zn- Fe_2O_4 is a soft magnetic material, and when Zn^{2+} in $Zn-Fe_2O_4$ is substituted by Mn^{2+} ions, there is a severe change in the magnetic properties such saturation magnetization (M_s), remanent magnetization (M_r) and coercivity (H_c) as illustrated in figure 4 (a-b).

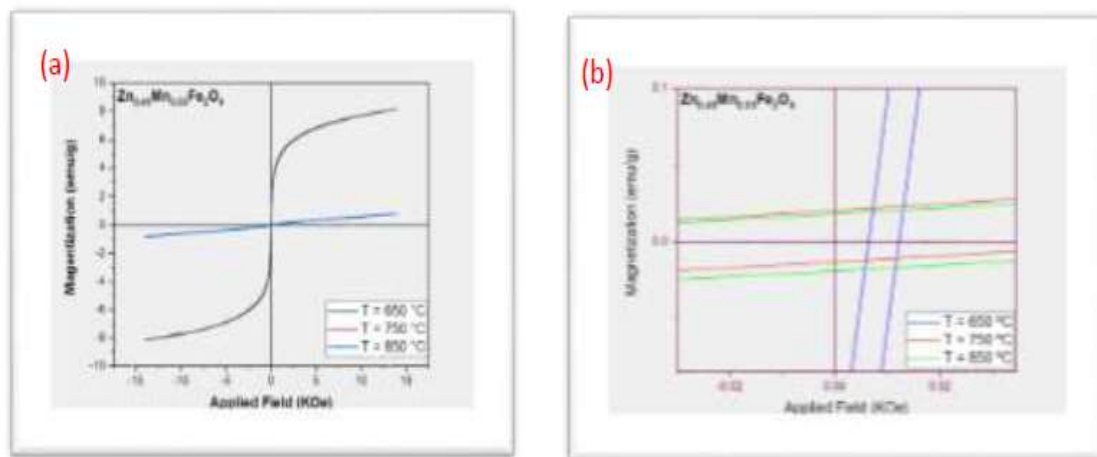


Figure 4 (a-b): VSM analysis of Zn_{0.45}Mn_{0.55}Fe₂O₄ ferrite nanocomposites at different calcination temperatures (650, 750, and 850 °C).

Table (2): VSM measurements of Zn_{0.45}Mn_{0.65}Fe₂O₄ nanocomposite with different content of zinc metal at different calcination temperatures (650, 750, and 860) °C.

3.4 LCR Meter

3.4.1 Dielectric Constant

Figures (5) show the temperature dependence of the dielectric constant (ϵ') for Zn_xMn_{1-x}Fe₂O₄ ferrite at four fixed frequencies (200 KHz, 500 kHz, 1 MHz, 1.5 MHz and 2 MHz). The (ϵ') increases with temperature at all frequencies, as can be seen in the graph. A rise in dielectric constant and loss as a function of rising temperature [18-19]. There are four distinct ways in which the dielectric constant of ferrite material can be attributed: interfacial, dipolar, electronic and ionic. Low-frequency polarizations, such as interfacial and dipolar, are very temperature dependent. The buildup of charge carriers at the grain boundary causes interfacial polarization. Charge carriers (electrons and holes) become more thermally activated and wander faster when the temperature rises. A rise in dielectric constant with rising temperature is a result of the increased electron hopping caused by this [20]. When capacitance (C) is measured using this equation, the value of r can be determined.

$$\epsilon' = Cd/\epsilon_0 A \dots\dots\dots(1)$$

where 'C' is capacitance (F), 'd' is the thickness of the dielectric/separation between the plates of the capacitor (m), ' ϵ_0 ' is the permittivity of free space ($\epsilon_0=8.85 \times 10^{-12}$ F m⁻¹) and 'A' is the area of the electrode (m²) [18].

Temp	H _c (Oe)	M _r (emu/g)	M _s (emu/g)	M _r /M _s	n _B (μB)	K (emu.Oe.g ⁻¹)
650	71	0.01	0.81	0.0218	0.029	60
750	27	0.95	9.39	0.1012	0.334	26
850	75	0.02	0.80	0.0286	0.029	63

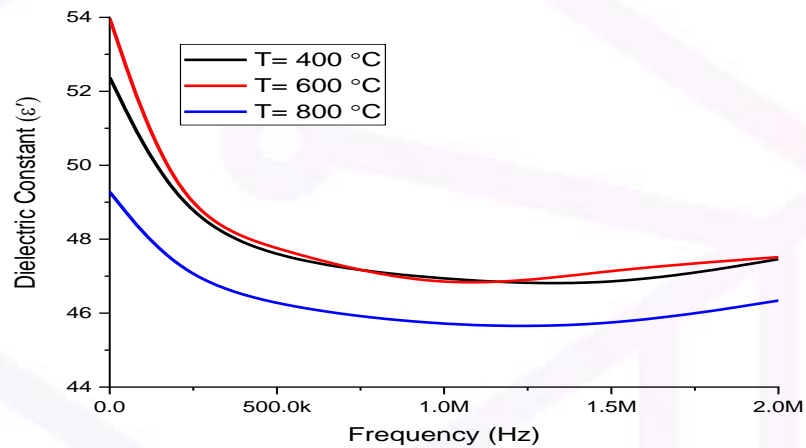


Figure (5): LCR meter a Frequency dependence of real part (ϵ') of $\text{Zn}_{0.45}\text{Mn}_{0.55}\text{Fe}_2\text{O}_4$ ferrite nanocomposites at different calcination temperatures (400, 600, 800 °C).

3.4.2 Dielectric Loss

It is the imaginary component of the dielectric constant (ϵ''), which is obtained from conductance (G) measured experimentally, that represents the energy absorbed by the sample when subjected to an external applied field.

$$\epsilon'' = Gd/\epsilon_0 A\omega \dots \dots \dots (2)$$

Where ($\omega = 2\pi f$) is the angular frequency and G is conductance, which is the reciprocal of resistance R. The standard unit of G is Siemens (S). The variation in ϵ'' with frequency from 200 KHz to 2 MHz at different temperatures from 400, 600, and 800 °C for (Mn-Zn-Fe₂O₄) samples is shown in figure (6) and table (3) [20].

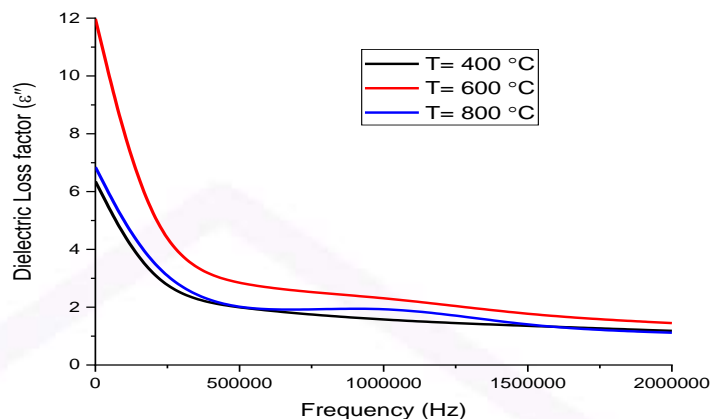


Figure (6): LCR meter variation of (ϵ'') with f (Hz) of $\text{Zn}_{0.45}\text{Mn}_{0.55}\text{Fe}_2\text{O}_4$ ferrite nanocomposites at different calcination temperatures (400, 600, 800 °C).

3.4.3 Dielectric Loss ($\tan \delta$)

Figure (7) and table (3) shows the change in $\tan \delta$ for ($\text{Zn}_x\text{Mn}_{1-x}\text{Fe}_2\text{O}_4$) composite samples at the concentrations ($x = 0.45$), correspondingly with applied frequencies ranging from (200 to 2) MHz and temperatures ranging from 400, 600, and 800 °C. At 200 Hz, the plots in the inset revealed the change in ($\tan \delta$). T , which suggested a drop in $\tan \delta$ with the increase in T ($\tan \delta$) began to drop with rising frequency and became linear at its lowest values for all samples at higher frequencies. Since the polarizability of ($\text{Zn}_x\text{Mn}_{1-x}\text{Fe}_2\text{O}_4$) composites increased with temperature, the value of \tan decreased, indicating that the energy retained was greater than the energy lost [21].

$$\tan \delta = \epsilon''/\epsilon' \dots\dots\dots(3)$$

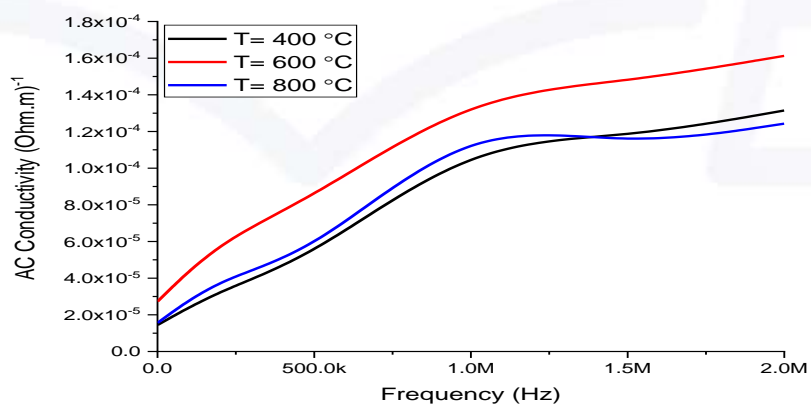


Figure (7): The AC conductivity of $\text{Zn}_{0.45}\text{Mn}_{0.55}\text{Fe}_2\text{O}_4$ ferrite nanocomposites at different calcination temperatures (400, 600, 800 °C).

Table (3): LCR measurements the dielectric parameters (ϵ''), (ϵ'), ($\tan \delta$) and (σ_{ac}) of $Zn_{0.45}Mn_{0.55}Fe_2O_4$ nanocomposite with at different calcination temperatures (400, 600, and 800) °C.

Frequency	Dielectric Parameters	400 °C	600 °C	800 °C
200 KHz	ϵ'	48.69	48.6	47.03
	ϵ''	2.47	3.74	2.97
	$\tan \delta$	0.05	0.08	0.06
	$\sigma_{ac} \times 10^{-5}$	3.36	6.06	4.04
500 KHz	ϵ'	47.39	47.7	46.16
	ϵ''	1.93	2.65	1.69
	$\tan \delta$	0.04	0.06	0.04
	$\sigma_{ac} \times 10^{-5}$	5.18	8.42	5.36
1 MHz	ϵ'	46.89	46.6	45.63
	ϵ''	1.54	2.37	2.15
	$\tan \delta$	0.03	0.05	0.047
	$\sigma_{ac} \times 10^{-5}$	1.15	0.14	0.13
1.5 MHz	ϵ'	46.70	47.2	45.63
	ϵ''	1.35	1.70	1.29
	$\tan \delta$	0.03	0.04	0.03
	$\sigma_{ac} \times 10^{-5}$	1.17	0.15	0.11
2 MHz	ϵ'	47.46	47.5	46.34
	ϵ''	1.18	1.45	1.12
	$\tan \delta$	0.02	0.03	0.02
	$\sigma_{ac} \times 10^{-5}$	1.31	0.161	0.124

4. Conclusion

In order for nanomaterials made by the sol-gel method to be used, they must be able to control the structural (XRD, and FE-SEM), magnetic (VSM), and electrical (LCR) properties of the Mn-Zn-ferrites nanocomposite. The NPs must be able to do this. This article talks about an investigation into the possibility of making Mn-Zn-ferrites (NPs) through sol-gel as possible nanomaterials that can be changed in shape. There were three types of tests that were used to look at the structure and magnetic properties of the Mn-Zn-ferrites that were made by the sol-gel

method. Ferrites have crystallites that are 27 to 30 nm in size, and XRD shows that the structure of the ferrites is cube-shaped (NPs). A lot of nanoparticles with a particle size of 25 to 40.2 nm were found in the forged Mn-Zn-ferrites that were made. Results from the VSM show that the magnetic nature of materials changed dramatically when Mn-Zn-ferrites nanoparticles were added to them. As magnetization and coercivity rose, the magnetic nature of the materials changed. A good magnetic parameter value ($M_s = 0.80$ emu/g and $H_c = 75$ Oe) at (850) °C was also found.

The Conflict of Interest

No conflict of interest.

Reference

1. Wu, W., Dey, D., Memis, O. G., Katnelson, A., & Mohseni, H., *Nanoscale Res. Lett.*, (2008) 3, 123.
2. Herlekar, M., Barve, S., & Kumar, R., *Plant-mediated green synthesis of iron nanoparticles. Journal of Nanoparticles*, 2014.
3. Issa, B., Obaidat, I., Albiss, B., & Haik, Y., *Magnetic Nanoparticles: Surface Effects and Properties Related to Biomedicine Applications. International Journal of Molecular Sciences*, (2013) 14(11), 21266–21305. doi:10.3390/ijms141121266.
4. Guo, J., Wang, R., Tjiu, W. W., Pan, J., & Liu, T., *Synthesis of Fe nanoparticles@ graphene composites for environmental applications. Journal of Hazardous Materials*, (2012) 225, 63–73.
5. Cornell RM, Schwertmann U. *The Iron Oxides: Structure, Properties, Reactions, Occurrences and Uses*. 2nd ed. John Wiley & Sons; 2006.
6. Abid, M. A., Kadhim, D. A., & Aziz, W. J. (2020). Iron oxide nanoparticle synthesis using trigonella and tomato extracts and their antibacterial activity. *Materials Technology*, 1-8.
7. Giri, A., Goswami, N., Sasmal, C., Polley, N., Majumdar, D., Sarkar, S., Bandyopadhyay, S.N., Singha, A., Pal, S.K.: Unprecedented catalytic activity of Mn_3O_4 nanoparticles: potential lead of a sustainable therapeutic agent for hyperbilirubinemia. *RSC Adv.* 4(10), 5075–5079 (2014)
8. Pal, M., Lee, S., Kwon, D., Hwang, J., Lee, H., Hwang, S., Jeon, S.: Direct immobilization of antibodies on Zn-doped Fe_3O_4 nanoclusters for detection of pathogenic bacteria. *Anal. Chim. Acta* 952, 81–87 (2017)



9. Hastings, J.M., Corliss, L.M.: Neutron diffraction study of manganese ferrite. *Phys. Rev.* 104, 328–331 (1956)
10. Elfalaky, A., Soliman, S.: Theoretical investigation of MnFe_2O_4 . *J. Alloys Compd.* 580, 401–406 (2013)
11. Li, J., Yuan, H., Li, G., Li, Y., Leng, J.: Cation distribution dependence of magnetic properties of sol–gel prepared MnFe_2O_4 spinel ferrite nanoparticles. *J. Magn. Mater.* 322, 3396–3400 (2010)
12. Pradhan, P., Giri, J., Samanta, G., Sarma, H.D., Mishra, K.P., Bellare, J.R., Banerjee, R., Bahadur, D.: Comparative evaluation of heating ability and biocompatibility of different ferrite based magnetic fluids for hyperthermia application. *J. Biomed. Mater. Res. B* 81B, 12–22 (2007)
13. Pal, M., Singh, A.K., Rakshit, R., Mandal, K.: Facile functionalization of Fe_2O_3 nanoparticles to induce inherent photoluminescence and excellent photocatalytic activity. *Appl. Phys. Lett.* 104, 233110 (2014)
14. Pal, M., Kundu, A., Rakshit, R., Mandal, K.: Surface chemistry modulated introduction of multifunctionality within Co_3O_4 nanocubes. *RSC Adv.* 5(21), 16311–16318 (2015)
15. Abdullah, M. Z., Al-Timimi, M. H., Albanda, W. H., Dumitru, M., Balan, A. E., Ceaus, C., ... & Stamatina, I. (2019). Structural And Electrochemical Properties Of $\text{P}_3\text{-Na}_0.67\text{mn}_0.3\text{co}_0.7\text{o}_2$ Nanostructures Prepared By Citric-Urea Self-Combustion Route As Cathode For Sodium Ion Battery. *Digest Journal Of Nanomaterials And BIOSTRUCTURES*, 14(4), 1179-1193.
16. Rath, C., Anand, S., Das, R. P., Sahu, K. K., Kulkarni, S. D., Date, S. K., & Mishra, N. C. (2002). Dependence on cation distribution of particle size, lattice parameter, and magnetic properties in nanosize Mn–Zn ferrite. *Journal of Applied Physics*, 91(4), 2211-2215.
17. Varshney, D., Verma, K., & Kumar, A. (2011). Structural and vibrational properties of $\text{Zn}_x\text{Mn}_{1-x}\text{Fe}_2\text{O}_4$ ($x = 0.0, 0.25, 0.50, 0.75, 1.0$) mixed ferrites. *Materials Chemistry and Physics*, 131(1-2), 413-419.